Inorganic Chemistry

Article

pubs.acs.org/IC

Crystal Growth and First Crystallographic Characterization of Mixed Uranium(IV)−Plutonium(III) Oxalates

Christelle Tamain,[†] Bénédicte Arab Chapelet,[†] Murielle Rivenet,*[,‡] Francis Abraham,[‡] Richard Caraballo,[§] and Stéphane Grandjean[†]

[†]CEA, Marcoule Research Center, DEN/DRCP/SCPS/LCCA, F-30207 Bagnols sur Cèze, France

[‡]Université Lille Nord de France, Unité de Catalyse et de Chimie du Solide, UCCS, UMR CNRS 8181, ENSCL-USTL, BP 90108, 59652 Villeneuve d'Ascq Cedex, France

[§]CEA, Marcoule Research Center, DEN/DTCD/SECM/LMPA, F-30207 Bagnols sur Cèze, France

Supporting Information

ABSTRACT: The mixed-actinide uranium(IV)−plutonium(III) oxalate single crystals $(NH_4)_{0.5}[Pu^{III}_{0.5}U^{IV}_{0.5}(C_2O_4)_2\cdot H_2O]\cdot nH_2O$ (**1**) and $(NH_4)_{2.7}Pu^{III}_{0.7}U^{IV}_{1.3}(C_2O_4)_5\cdot nH_2O$ (**2**) have been prepared by the diffusion of different ions through membranes separating compartments of a triple cell. UV−vis, Raman, and thermal ionization mass spectrometry analyses demonstrate the presence of both uranium and plutonium metal cations with conservation of the initial oxidation state, U^{IV} and Pu^{III}, and the formation of mixed-valence, mixed-actinide oxalate compounds. The structure of **1** and an average structure of **2** were determined by single-crystal X-ray diffraction and were solved by direct methods and Fourier difference techniques. Compounds **1** and **2** are the first mixed uranium(IV)−plutonium(III) compounds to be structurally characterized by single-crystal X-ray diffraction. The structure of **1**, space group *P*4/*n*, a = 8.8558(3) Å, b = 7.8963(2) Å, Z = 2, consists of layers formed by four-membered rings of the two actinide metals occupying the same crystallographic site connected through oxalate ions. The actinide atoms are nine-coordinated by oxygen atoms from four bidentate oxalate ligands and one water molecule, which alternates up and down the layer. The single-charged cations and nonbonded water molecules are disordered in the same crystallographic site. For compound **2**, an average structure has been determined in space group *P*6/*mmm* with a = 11.158(2) Å and c = 6.400(1) Å. The honeycomb-like framework $[Pu^{III}_{0.7}U^{IV}_{1.3}(C_2O_4)_5]^{2.7-}$ results from a three-dimensional arrangement of mixed $(U_{0.65}Pu_{0.35})O_{10}$ polyhedra connected by five bis-bidentate μ^2-oxalate ions in a trigonal-bipyramidal configuration.

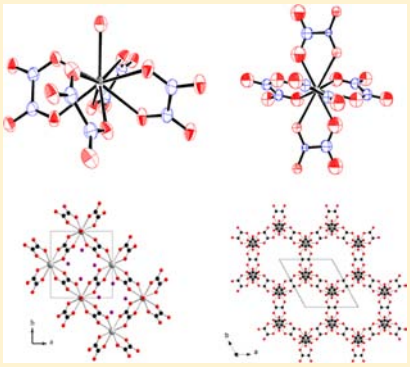

INTRODUCTION

Because of the role of oxalic acid in actinide processing in the nuclear fuel cycle, the interaction of oxalate ions with actinides in aqueous solution or in the formation of solid compounds is of interest and requires further investigation. Oxalic acid is used to recover actinides from spent nuclear fuel thanks to the very low solubility of actinide(IV) and actinide(III) oxalate compounds even in acidic solution.[1] While numerous simple and double oxalates of thorium(IV),[2−5] uranium(IV),[5−9] uranium(VI) (UO_2^{2+} ion),[10,11] and neptunium(V) (NpO_2^{+} ion)[12] have been structurally characterized, in spite of their interest, very few structural characterizations by single-crystal X-ray diffraction (XRD) of transuranium(IV or III) (TRU) oxalates have been carried out to date, and their structures were often compared to those of uranium(IV) and thorium(IV) for the actinide(IV) compounds and to those of lanthanide(III) for the actinide(III) compounds.[13,14] Concerning the simple actinide(IV) oxalates belonging to the $An^{IV}(C_2O_4)_2\cdot 6H_2O$ series, the structure has been determined for An = U[7] and Np[15] but not for An = Pu despite its industrial interest, because it is the phase formed during the PUREX process, leading to PuO_2 after decomposition in which the Pu^{IV}/Pu^{III} redox phenomena occur.[16] For the dihydrate $An^{IV}(C_2O_4)_2\cdot 2H_2O$, the structures are known only for An = Th and U[5]. $An^{IV}(C_2O_4)_2(H_2O)_2\cdot 2H_2O$ has been obtained only for An = Th by in situ oxalate synthesis.[3] With a monovalent cation, three actinide(IV)-containing structures have been reported. The structure of $(H_3O)_2Np^{IV}_2(C_2O_4)_5\cdot nH_2O$ has been determined in a hexagonal cell with a = 11.001(1) Å and c = 6.333(2) Å.[17] That of $(NH_4)_2U^{IV}_2(C_2O_4)_5\cdot nH_2O$ was subsequently determined in a larger cell $a' \approx a\sqrt{3}$ and $c' \approx 2c$, leading to a better description of the three-dimensional (3D) actinide oxalate framework.[8] The structure of $K_4An^{IV}(C_2O_4)_4\cdot 4H_2O$ with An = U[4] and Th[2] is based on $[An(C_2O_4)_4]^{4-}$ chains that are present in the $\{C(NH_2)_3\}_4[An^{IV}(C_2O_4)_4\cdot 2H_2O]$ series recently described for An = U, Th, Pu, and Np.[18] A plutonium(IV) oxalate containing hydroxide anions, $KPu(C_2O_4)_2(OH)\cdot 2H_2O$, was recently characterized by Runde et al.[19] The same authors have also

Received: November 27, 2012
Published: April 11, 2013

synthesized and studied single crystals of the plutonium(III) oxalate $Pu^{III}_2(C_2O_4)_3(H_2O)_3{\cdot}6H_2O$,[19] isomorphic with $Ln_2(C_2O_4)_3(H_2O)_3{\cdot}7H_2O$.[20] The 50 years between the structure determinations of these last two compounds highlight the difficulties in synthesizing far more elaborate actinide single crystals and in resolving their structure. These crystallographic studies of actinide(IV) and actinide(III) oxalates indicate the high diversity of coordination polyhedra of the central atom (with three to five oxalate ligands and zero to three water molecules) as well as the numerous topologies and overall arrangements of the structure due to the multiplicity of the coordination modes of the oxalate ligands.[21] The dimensionality of the metal oxalate arrangement varies as well with structures based on chains, layers, or the 3D network.

Oxalic coprecipitation is a particularly convenient means for actinide conversion into oxalate compounds, suitable precursors of mixed-actinide oxide solid solutions (possible fuels for generation III/IV reactors).[22−24] The microstructures and properties of the mixed oxides depend mainly on the microstructures of the oxalate precursors, which is correlated with its structure, with the oxalate decomposition being generally morphotropic.[23,25,26] To the best of our knowledge, there is no structural study concerning mixed-valence (III and IV), mixed-actinide compounds, with XRD analyses being limited to structure identification using powder XRD.[25] The reference patterns are based on uranium(IV)−lanthanide(III) systems considered to be good crystallographic analogues of actinide(IV)−actinide(III) systems according to their similar ionic radii.[27,28] Three mixed uranium(IV)−lanthanide(III) oxalate series, named *hexagonal*, *triclinic*, and *tetragonal*, with the formula $M_{2+x}U^{IV}_{2-x}Ln^{III}_x(C_2O_4)_5{\cdot}nH_2O$ for the first and $M_{1-x}[Ln^{III}_{1-x}U^{IV}_x(C_2O_4)_2{\cdot}H_2O]{\cdot}nH_2O$ for the last two, were recently reported,[8,29,30] where M is a monovalent cation. These three structural series are characterized by a mixed crystallographic site, which accommodates both U^{IV} and Ln^{III} ions despite their charge difference. The charge compensation due to substitution of the trivalent cation for the tetravalent cation, or vice versa, is ensured by the presence of single-charged cations M located in the interspaces of the structure. The possibility of precipitating actinide(IV)−actinide(III) oxalate powders that belong to the hexagonal and tetragonal series has been shown.[22,24,25] Because previous papers have demonstrated that the structural behavior depends on the $An^{IV}/An^{III}/M^+$ system under consideration,[22,25] crystallographic studies on the An^{IV}/An^{III} systems of interest instead of analogues appear necessary. Besides, although lanthanides are often considered to be surrogates of actinides, many studies showed that their chemistry and their structural chemistry could sometimes differ both between lanthanide(III) and actinide(III)[31,32] and between cerium(IV), thorium(IV), uranium(IV), and transuranic actinide(IV).[33]

Recently, we have demonstrated the efficiency of crystal growth of transuranium oxalates by the slow diffusion of different reagents through membranes in a specially designed diffusion cell.[34] This synthesis route is dedicated to these elements and their particular chemistry (hydrolysis, redox chemistry, etc.). The use of this crystal growth method for the $U^{IV}/Pu^{III}/NH_4^+$ system enabled us to isolate two types of mixed uranium and plutonium oxalate single crystals, $(NH_4)_{0.5}[Pu^{III}_{0.5}U^{IV}_{0.5}(C_2O_4)_2{\cdot}H_2O]{\cdot}nH_2O$ (**1**) and $(NH_4)_{2.7}Pu^{III}_{0.7}U^{IV}_{1.3}(C_2O_4)_5{\cdot}nH_2O$ (**2**). The preparation, characterization by thermal ionization mass spectrometry (TIMS) analysis and UV−vis and Raman spectroscopy, and structural study by XRD of these oxalates are reported in this paper.

EXPERIMENTAL SECTION

Reagents. Because of the radioactive nature of the actinides, especially plutonium, the experiments were carried out in gloveboxes with very restrictive protocols. Uranium(IV) and plutonium(III) solutions were prepared separately using specific procedures, either from purified monometallic solutions or by dissolving monometallic oxides or hydroxides. The uranium(IV) nitrate solution is prepared by the catalytic reduction of a uranium(VI) nitrate solution from Areva (natural uranium) by dihydrogen on a platinum/silicon backing. The plutonium(IV) solution is prepared by dissolving the corresponding oxide PuO_2 with concentrated HNO_3 in a glovebox. The plutonium(III) solution is prepared by the reduction of the plutonium(IV) solution by hydrazinium nitrate ($N_2H_5^+$ and NO_3^-). The concentration of actinides in these primary solutions is close to 1 mol·L^{-1}. Hydrazinium nitrate was also used as an antinitrous agent to stabilize the lowest oxidation states (typically IV for uranium and III for plutonium). The concentration, purity, and oxidation state were determined by UV−vis absorption spectroscopy of the solutions. In the uranium(IV) or plutonium(III) solutions, the concentration of hydrazinium cations is around 0.2 mol·L^{-1}.

Synthesis. The oxalate single crystals were prepared by diffusion of the different species through membranes in a three-compartment cell[34] (compartments separated by membranes; Figure 1). Among the different existing membranes (pseudoliquid, functionalized polymer, and ceramic membranes), compressed glass fiber membranes (Whatman GF/F, thickness of 0.7 μm) were chosen because they are nonselective and highly stable in acidic media and do not need preliminary synthesis.

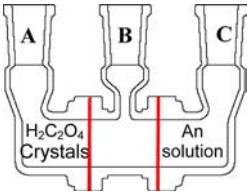

Figure 1. Scheme of the three-compartment diffusion cell.

A nitric acid solution of 0.01 mol·L^{-1} of uranium(IV) and 0.01 mol·L^{-1} of plutonium(III) was placed in the compartment (C), whereas crystals of oxalic acid were placed in the opposite compartment (A) in an acidic nitrate medium. The three compartments were filled with nitric acid (1.5 mol·L^{-1}) and ammonium ($[NH_4^+]$ = 1 mol·L^{-1}), introduced as ammonium nitrate, so as to fix these concentrations throughout the cell; therefore, compartment B only contained the ammonium solution ($[NH_4^+]$ = 1 mol·L^{-1}) in an acidic nitrate medium. With the concentration of ammonium nitrate in the initial solution being more important than that of hydrazinium, ammonium ions likely play the role of charge compensator. Solids appear after 3 days in the three compartments. Their nature and composition vary along the diffusion cell. In compartment A, a powder and crystals of type **1** are mainly formed, whereas in compartment C, a powder and crystals of type **2** are principally obtained. In the intermediate compartment, only powder is formed. The solid is filtered off and dried at room temperature without any wash. The selective synthesis of crystals **1** and **2** in the different compartments can be due to the gradient of the oxalic acid concentration along the triple cell.[34] Crystals are separated from the powder thanks to a needle.

Characterizations. *Single-Crystal XRD Studies.* To prevent plutonium health hazards, each crystal was mounted on MicroMount patented by MiTeGen, inserted into a goniometer base. A MicroRT capillary was then drawn over the sample and onto the base, where it was sealed by adhesive. The single-crystal XRD intensities were measured on a Nonius four-circle diffractometer equipped with an Apex II charge-coupled device at 150 K using a 600 series cryostream

dx.doi.org/10.1021/ic302587t | *Inorg. Chem.* 2013, 52, 4941−4949

Table 1. Summary of Crystallographic Data Collection and Structure Refinement for 1 and 2

	1	2
formula	$(NH_4)_{0.5}$ $[Pu^{III}_{0.5}U^{IV}_{0.5}(C_2O_4)_2{\cdot}H_2O]{\cdot}nH_2O$	$(NH_4)_{2.7}$ $Pu^{III}_{0.7}U^{IV}_{1.3}(C_2O_4)_5{\cdot}nH_2O$
cryst size, μm	square plates, 150 × 150 × 20	hexagonal tubes, 200 × 40 × 40
cryst syst	tetragonal	hexagonal
space group	*P4/n*	*P6/mmm*
a, Å	8.8558(6)	11.158(2)
c, Å	7.8963(2)	6.400(1)
volume, Å^3	619.27(2)	690.1(2)
Z	2	1
R(int)	0.0212	0.0257
final *R* indices $[I > 2\sigma(I)]$ (R, R_w)	0.0198, 0.0242	0.0419, 0.0525
R indices (all data) (R, R_w)	0.0191, 0.0242	0.0419, 0.0525

cooler (Oxford Cryosystem). The instrument was equipped with a fine-focus Mo-target X-ray tube (λ = 0.71073 Å) operated at 1500 W. A hemisphere of data was collected using ω scans, with 30 s frame exposure and 0.5° frame widths. Intensities were extracted from the collected frames using the program *SAINTPlus*.[35] The lattice parameters were refined from the complete data set, and an empirical absorption correction was performed.[36] The particular shape of crystal **2** (hexagonal tubes) was not taken into account in the geometric absorption correction. This could be one reason, with disorder, why the reliability factors (see Table 1) and the estimated standard deviations on the intensity-dependent parameters are higher than those for crystals **1**. The structure determination and refinement were performed with *JANA2000* software.[37] The heavy atoms were located by direct methods using *SIR97*,[38] while the remaining atoms were found from successive Fourier map analyses. For crystal **1**, the structure refinement considered the two actinide ions (U^{IV} and Pu^{III}) in the same crystallographic site half-occupied by each atom in agreement with the TIMS analyses. The mixed U/Pu site thermal ellipsoid is slightly elongated in the [0 0 1] direction. Splitting the position of the two heavy atoms on two sites allows a very weak reduction in the reliability factors (R = 0.0178, R_w = 0.253 $[I > 2\sigma(I)]$ and R = 0.0186, R_w = 0.253 [all data]), and the consequences on the An−O distances are discussed below. All of the non-hydrogen atoms were located, and their positions were refined anisotropically. The location of the hydrogen atoms of the water molecules or single-charged ions was not determined because of the presence of very heavy atoms and significant thermal agitation of these molecules. The principal crystal data and details of the final refinement are reported in Tables 1 and S1−S3 in the Supporting Information. For crystal **2**, the structure was solved in a hexagonal cell with parameters a = 11.158(2) Å and c = 6.400(1) Å close to the unit cell used for the crystal study of $(H_3O)_2Np^{IV}_2(C_2O_4)_5{\cdot}nH_2O$ with a = 11.001(1) Å and c = 6.333(2) Å.[17] However, a better solution has been obtained in the hexagonal space group *P6/mmm* instead of trigonal *P*3. As for crystal **1**, the U^{IV} and Pu^{III} atoms fully occupy the same crystallographic site with the occupation factor fixed to the value deduced from the TIMS analyses.

Powder XRD. Powder XRD data were obtained with a Bruker AXS D8 diffractometer (curved position-sensitive detector) using Cu radiation ($K\alpha_1$ = 1.5406 Å; $K\alpha_2$ = 1.5444 Å) and mounted with a LynxEye angular detector. The scan step was 0.02° with a counting time of 0.5 s·step^{-1} from 5° to 60°. Silicon was added to all samples as an internal standard to calibrate the angular positions of the observed XRD lines. The oxalate compounds and silicon were mixed with an epoxy resin to prevent contamination spreading. $K\alpha_2$ stripping of the Cu radiation according to the Rachinger method, as well as the baseline and angle shift corrections, was performed by empirical calculations and *EVA* software.[39] The amount of solid formed in the different compartments is too small to allow characterization compartment by compartment. Thus, the solids formed in the three compartments were mixed, leading to an adequate amount of powder for global analysis. The X-ray diagram was compared to the $An^{IV}(C_2O_4)_2{\cdot}6H_2O$ experimental pattern and to the compound **1** and **2** XRD patterns calculated from single-crystal structure determination results.

Raman Microspectroscopy. A Jobin−Yvon LabRam Raman spectrometer was used in conjunction with a nuclearized microscope (Optique Peter, Lyon, France) with an objective turret (1.25×, 5×, 10×, 20×, 50×, and 100×). A YAG laser (532 nm) with output power adjustable from 20 to 120 mW was used with a variable filter to provide low-excitation-beam power levels. The optical microscope was mounted in a hot cell, while the Raman spectrometer and laser were installed outside the cell with a fiber-optic signal transmission line. The microscope objective used for oxalate single-crystal analyses was 20×. For both crystals, five different crystals were analyzed and the results averaged.

TIMS Analyses. TIMS analyses were performed on a solution prepared by dissolution of a dozen single crystals of each type (selected and separated from the powder with a needle) in 125 μL of a 8 mol·L^{-1} nitric acid solution. Before analysis, the solution was diluted by adding water until the concentration of nitric acid was equal to 1 mol·L^{-1}. A VG-54 magnetic sector mass spectrometer was used. An internal standard of known isotopic composition and concentration was added to the sample. Finally, the actinide content could be determined from the measured final sample concentrations and the known internal standard concentration.

UV−Vis Spectroscopy. The actinide concentrations in solution were determined by UV−vis absorption spectroscopy using a GBC Cintra 10e UV spectrophotometer between 350 and 900 nm by deconvolution of the spectra using reference spectra of actinide solutions with known concentrations previously recorded in the same conditions. It was not possible to use the molar extinction coefficients of actinide in nitric acid media given in the literature because of the specific analysis conditions with long glass fibers between the spectrometer and sample located in a glovebox. The actinide oxidation states in the precipitates were investigated in a glovebox using a Hitachi U-3000 spectrophotometer equipped with an integration sphere for reflection measurements. Considering the amount of solid needed to perform analyses, the data were collected using a mixture of solids coming from the three compartments.

RESULTS AND DISCUSSION

Crystals **1**, gray-purple square plates of size suitable for single-crystal XRD, are mainly formed in compartment A, whereas crystals **2**, green hexagonal tubes, are principally grown in compartment C (Figure 2). However, they are always accompanied by some crystals of the second type and powder. In a previous paper on single-crystal growth of actinide oxalates using a diffusion cell, a mechanism to explain the formation of the unexpected shape of crystals **2** has been proposed.[34]

Although there are some preferential locations of the two types of single crystals in the cell compartments, segregation is not complete, and the powder XRD analyses were carried out on the whole solid formed in the diffusion cell (Figure 3). The signature of an oxalate phase that pertains to the *hexagonal*

dx.doi.org/10.1021/ic302587t | Inorg. Chem. 2013, 52, 4941−4949

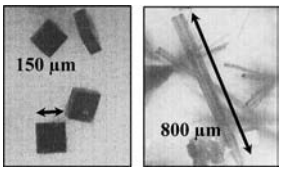

Figure 2. Single crystals of mixed uranium(IV)−plutonium(III) oxalates with square-plate (**1**) and hexagonal-tube (**2**) shapes.

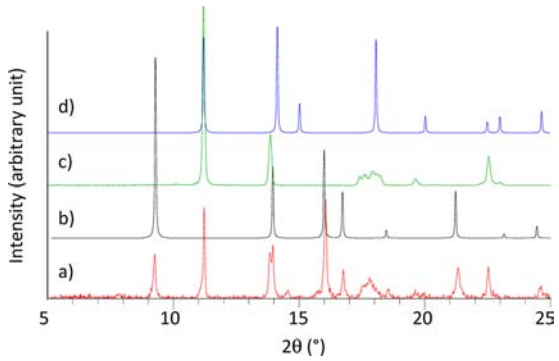

Figure 3. XRD pattern of the solid formed in the three-compartment cell (a) compared to the experimental uranium(IV) oxalate hexahydrate pattern (c) and the XRD patterns calculated from the results of the crystal structure determinations of crystals **1** (d) and **2** (b).

series[8] (2θ = 9°, 14°, 16°, 16.5°, and 21°) clearly appears on the XRD pattern. The broad reflections at 2θ = 17.5° are characteristic of the uranium(IV) oxalate hexahydrate experimental pattern; furthermore, the two components of the double peak at 2θ = 13.8/13.9° correspond respectively to uranium(IV) oxalate hexahydrate[7] and the *hexagonal* oxalate. The presence of a *tetragonal*-type phase[30] was not evidenced in the powder XRD pattern. No uranium(IV) oxalate hexahydrate single crystal was found, showing that the powder accompanying the hexagonal tube and the square-plate crystals is constituted in the majority of $U(C_2O_4)_2{\cdot}6H_2O$.

TIMS analyses performed separately on both single crystals confirm the presence of uranium and plutonium in the two types of crystals. The plutonium represents for the square plates and hexagonal tubes respectively 50 ± 7% and 35 ± 9% of the total metallic cation amount. As it was already observed for powdered mixed-actinide oxalates,[8,22,25,30] the *tetragonal* series corresponds to a An^{III}/An^{IV} ratio higher than for the *hexagonal* series.

UV−vis analysis was carried out to determine the oxidation states of the two actinides in the solid (Figure 4). As described in the Experimental Section, the analyzed solid results from a mixture of the solids collected in the three compartments; it was not possible to discriminate the solids from compartment A, B, or C. The reflectance spectrum is compared, on the one hand, to the absorbance spectra of nitric acid solutions of uranium(IV) oxalate, uranium(VI) oxalate, plutonium(III) oxalate, and plutonium(IV) oxalate and, on the other hand, to the reflectance spectra of the solid uranium(IV) oxalate $M_2U^{IV}{}_2(C_2O_4)_5{\cdot}nH_2O$, solid plutonium(IV) oxalate $Pu^{IV}(C_2O_4)_2{\cdot}6H_2O$, and solid plutonium(III) oxalate $Pu^{III}{}_2(C_2O_4)_3{\cdot}9H_2O$, used as references and synthesized during this study by oxalic precipitation. The reflectance spectrum of Pu^{III} is characterized by the bands at 560 and 600 nm. This characteristic signature is observed on the reflectance spectrum of the studied solid, confirming the presence of trivalent plutonium. The minor shift of the wavelengths is due to different Pu^{III} coordination modes and thus to different environments in the solid. The supplementary band at 475 nm and the broad one at 650 nm confirm the presence of U^{IV}. The broadening of the band at 550 nm as well as the shoulder at the left of the band for the uranium(IV)−plutonium(III) solid are due to U^{IV} (Figure 4A). The reflectance spectrum of the solid has the same overall shape as the combination of the absorbance spectra of the uranium(IV) and plutonium(III) oxalate aqueous solutions with a broadening and a small shift of the major peaks to higher wavelengths. This property has already been discussed by Runde et al.[19] The absence of the sharp, intense band at 480 nm characteristic of Pu^{IV} confirms the absence of Pu^{IV}. In fact, the stability of Pu^{III} in time is only apparent because it can be oxidized by α-self-irradiation to Pu^{IV}, which immediately reacts with U^{IV} in a nitric acid medium through a redox reaction to form Pu^{III} and U^{VI}.[40] So as long as there is some U^{IV} in the solution, Pu^{IV} cannot exist. U^{VI}, if it exists, was not incorporated into the solid phase because uranium(VI) oxalate has a far higher solubility than plutonium(III) or uranium(IV) oxalate (the pK's are in the range 25−31 for Ln/An^{III},[41] in the range 21−23 for An^{IV},[42] and between 8

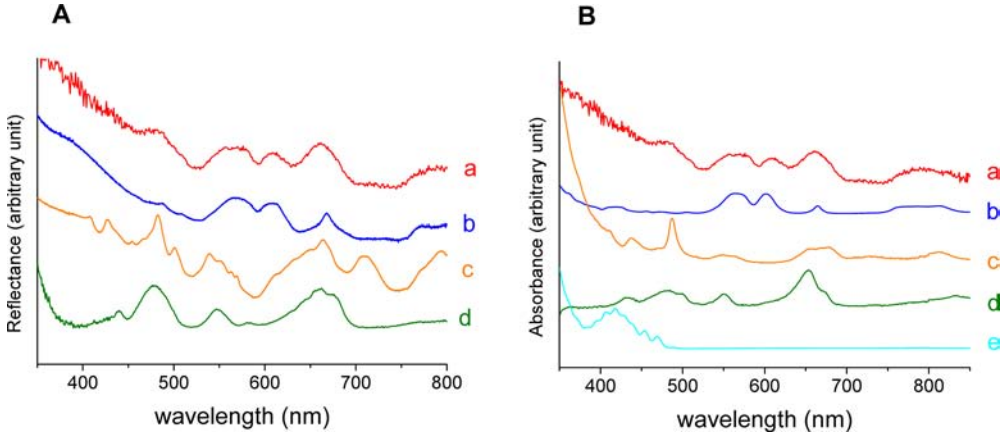

Figure 4. (A) UV−vis reflectance spectra of the solid obtained in the triple cell (a), $Pu^{III}{}_2(C_2O_4)_3{\cdot}9H_2O$ (b), $Pu^{IV}(C_2O_4)_2{\cdot}6H_2O$ (c), $M_2U^{IV}{}_2(C_2O_4)_5{\cdot}nH_2O$ (d). (B) UV−vis reflectance spectrum of the solid obtained in the triple cell (a) and absorbance spectra in nitric acid of Pu^{III} (b), Pu^{IV} (c), U^{IV} (d), and U^{VI} (e) in the presence of oxalic acid.

dx.doi.org/10.1021/ic302587t | Inorg. Chem. 2013, 52, 4941−4949

and 9 for An^{VI} [43]). The spectra (Figure 4B) confirm this statement because, besides the baseline deviation, the signature of the uranium(VI) oxalate complex is absent. UV−vis absorption and reflectance data show only the presence of U^{IV} and Pu^{III} in the total solid and so conservation of the initial oxidation state of plutonium and uranium.

The poor resolution of the micro-Raman spectra recorded separately on both single crystals is due (i) to the necessity of maintaining the samples in a hot cell while the Raman spectrometer and laser are installed outside the cell with a fiber-optic signal transmission line, (ii) to the small thickness of the single crystals, and (iii) to the low laser power used to avoid damaging the crystals. The micro-Raman spectra of both single-crystal types (Figure 5) are similar and in agreement with the literature devoted to natural oxalates.[44]

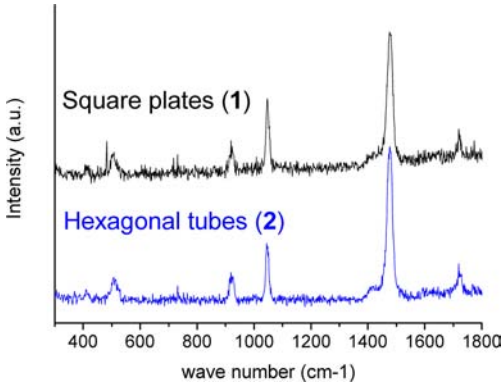

Figure 5. Micro-Raman spectra of the two types of single crystals.

The peak observed near 510 cm^{-1} is assigned to the δ(O−C−O) bending modes. The stretching of the C−C bond is correlated with the band recorded at around 920 cm^{-1}, while the band observed at 1480 cm^{-1} is attributed to the symmetric (ν_s) stretching mode of the C−O vibration. The band around 1720 cm^{-1} is attributed to the antisymmetric stretching mode of the C−O vibration in the presence of water and hydrogen bonds. The broad band at 1480 cm^{-1} reveals the existence of several distinct oxalate ions and can be explained by the possible presence of free oxalate molecules responsible for additional bands.[45] It could also be caused by different nonequivalent crystallographic oxalate groups in the unit cell.[5] For the tetragonal crystals (**1**), the latter hypothesis must be excluded because there is only one equivalent oxalate ligand and so the width of the band is probably due to free oxalates absorbed at the surface of the crystals. For the hexagonal tubes (**2**), it is more difficult to conclude because there are several nonequivalent oxalate ions in the unit cell.[8] It is also interesting to notice the wavenumber shift of this band, from 1477 cm^{-1} for the squares plates to 1487 cm^{-1} for the hexagonal tubes, underlining the different coordination modes of the oxalate groups in the two phases. The band observed at 1050 cm^{-1} is assigned to the symmetric stretching[46] of the nitrate groups probably absorbed at the surface of the crystals.

Crystallographic data and structure refinement parameters for **1** and **2** are given in Table 1.

The structure of **1** consists of a 2D actinide oxalate anionic framework. The structure contains one crystallographically independent metallic atom and one independent oxalate ligand. The actinide atoms are at the center of a pseudosquare pyramid; the square base is formed by four oxalates, and the axial position is occupied by a water molecule, creating a $[An(C_2O_4)_4(H_2O)]$ entity with a geometry similar to that of the isolated ion $[Ln(CO_3)_4(H_2O)]^{5-}$ observed in several lanthanide carbonates.[47,48] The actinide ions are coordinated by nine oxygen atoms forming a monocapped square antiprism $(U,Pu)O_9$ and eight oxygen atoms from four symmetrically related chelating bidentate oxalate anions, with the latter being the capping water oxygen atom O1 (Figure 6). For symmetry

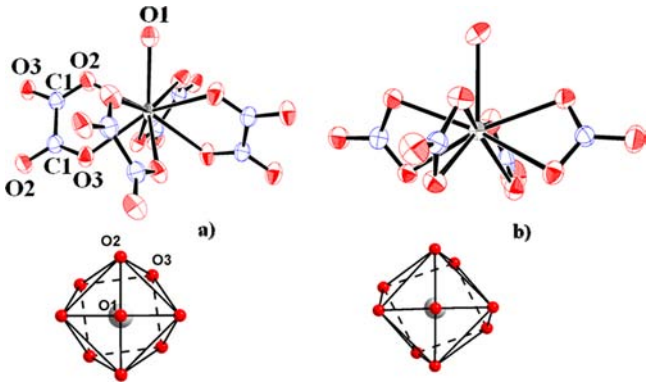

Figure 6. Comparison of (a) the $[An(C_2O_4)_4(H_2O)]$ entity and the mixed $U^{IV}/Pu^{III}O_9$ polyhedron in **1** with (b) the $[Nd(CO_3)_4(H_2O)]^{5-}$ ion and the NdO_9 polyhedron in $[C(NH_2)_3]_5[Nd(CO_3)_4(H_2O)]\cdot 2H_2O$.[47]

reasons, both O2 and O3 squares are parallel, with a distance between the two planes of 2.260 Å. The U/Pu ion is located at 0.7972(3) Å from the O2 plane and 1.4627(3) Å from the O3 plane. The twist angle 37.87(8)° is larger than the value found for the guanidinium neodymium(III) carbonate $[(C(NH_2)_3]_5[Ln(CO_3)_4(H_2O)]\cdot 2H_2O$[47] (23.2°); this can be explained by the larger distance between O2 and O3 chelating oxygen atoms in oxalate (about 2.67 Å) than in carbonate (about 2.21 Å), so the polyhedron gets closer to an ideal square antiprism. The An−O distances are comparable with the Nd−O distances (Table 2) except for the distances with the water oxygen atoms, which are significantly larger for Nd^{III} (M−O1; Table 2). This is often observed in complexes in which complexation by hard anions such as oxalate and carbonate allows a wide variation of other bond distances in the coordination polyhedron.[49] The pentagonal environment of Pu^{IV} ensured by four oxalates and one OH in the $[Pu(C_2O_4)_4(OH)]$ entity in $KPu(C_2O_4)_2(OH)\cdot 2H_2O$ moves away from a square pyramid, and the polyhedron PuO_9 is better described as a distorted tricapped trigonal prism.[19]

Bridging bis-bidentate μ^2-oxalate ions connect adjacent actinide atoms to form four-membered rings (Figure 7), exhibiting a square aperture of about 4.92 Å × 4.92 Å, leading to a 2D arrangement with layers stacked along the *c* axis (Figure 7). The distance between two actinide atoms from adjacent layers is equal to 7.8963(2) Å (*c* parameter). Analogous 2D polymeric structures with lanthanide or actinide metal in a monocapped square antiprism were already found in various double lanthanide oxalates $M[Ln(C_2O_4)_2(H_2O)]$,[50,30] in the uranium(IV) oxalate $U^{IV}(C_2O_4)_2\cdot H_2O\cdot$dma (dma = dimethylamine[7]), and in mixed uranium(IV)/lanthanide(III) oxalates.[30] In the monoclinic actinide oxalates $An^{IV}(C_2O_4)_2\cdot 6H_2O$ (An = Np[15] and U[7]) and $An^{IV}(C_2O_4)_2\cdot 2H_2O$ (An = Th and U[5]), the 2D actinide oxalate arrangements are similar but the actinide−oxygen polyhedra are, nevertheless, different with (i) no

dx.doi.org/10.1021/ic302587t | Inorg. Chem. 2013, 52, 4941−4949

Table 2. M−O (M = U, U/Nd, U/Pu, or Nd) Distances (Å) and Twist Angles (deg) for 1 Compared to $[U^{IV}(C_2O_4)_2{\cdot}H_2O]{\cdot}$dma, $(NH_4)_{0.4}[Nd^{III}_{0.4}U^{IV}_{0.6}(C_2O_4)_2(H_2O)]{\cdot}nH_2O$, and $[C(NH_2)_3]_5[Nd(CO_3)_4(H_2O)]{\cdot}2H_2O$[47]

	$[U^{IV}(C_2O_4)_2{\cdot}H_2O]{\cdot}$dma	$(NH_4)_{0.4}[Nd^{III}_{0.4}U^{IV}_{0.6}(C_2O_4)_2(H_2O)]{\cdot}nH_2O$	1	$[C(NH_2)_3]_5[Nd(CO_3)_4(H_2O)]{\cdot}2H_2O$[47]
M−O1	2.390(11) (1×)	2.494(7) (1×)	2.413(8) (1×)	2.694(4)[a]
M−O2	2.439(5) (4×)	2.451(3) (4×)	2.439(4) (4×)	2.465(4)[a]
M−O3	2.480(5) (4×)	2.485(3) (4×)	2.478(4) (4×)	2.506(3)[a]
⟨M−O⟩	2.452(5)	2.471(7)	2.453(8)	2.509(4)[a]
twist angle	38.6(1)	36.52(6)	37.87(8)	23.2[a]
d(M−plane O2)	0.7665(5)	0.8252(8)	0.7972(3)	0.7233(2)
d(M−plane O3)	1.4474(5)	1.4647(8)	1.4627(3)	1.3072(2)

[a]Average value.

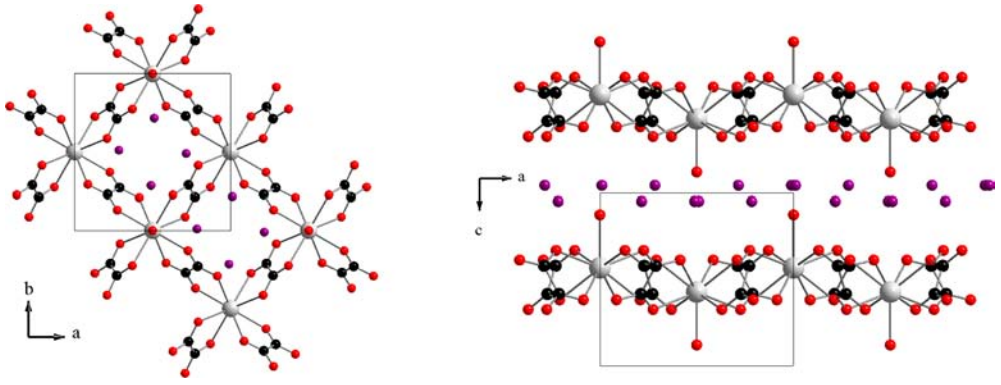

Figure 7. Projection in the (001) plane of the actinide oxalate layer showing the four-membered rings (left) and stacking of the layers along the *c* axis (right) in structure **1**.

bounded water molecule for $An^{IV}(C_2O_4)_2{\cdot}6H_2O$, a coordination number (CN) for U^{IV} of 8, and a cubic UO_8 polyhedron and (ii) two bounded water molecules for $An^{IV}(C_2O_4)_2{\cdot}2H_2O$, leading to a CN of 10 and a bicapped square antiprism. Thus, depending upon the number of coordinated water oxygen atoms, the CN of the actinide in this 2D actinide oxalate network increases from 8 to 10.

The bond lengths and angles in the common planar geometry of a bis-chelating oxalate ligand [the distance C−O ranges from 1.258(7) to 1.275(7) Å, C−C is 1.502(8) Å, the angle O−C−O is 127.04(1)°, and O−C−C ranges from 116.16(1) to 116.75(1)°] are in good agreement with the mean values reported by Hahn for oxalate compounds: C−O = 1.24 Å, C−C = 1.55 Å, O−C−O = 125°, and O−C−C = 117°[51] (Table S4 in the Supporting Information). The U/Pu−O distances vary over a narrow range from 2.413(8) to 2.478(4) Å, with the shorter distance being for the water oxygen atom O1. The average value [2.453(8) Å] is significantly shorter than that obtained for the plutonium(III) oxalate [2.518(8) Å].[7] This decrease can be due to the presence of U^{IV} in the actinide site, with U^{IV} having a smaller ionic radius than Pu^{III} ($R_{U^{IV}}$ = 1.05 Å[27] and $R_{Pu^{III}}$ = 1.165 Å[28] for CN = 9).

Charge compensation due to the substitution of trivalent ions for tetravalent ions is ensured by single-charged cations located in the interlayer space of the structure. It was difficult to clearly identify the species located in the interlayer space because they could be H_2O and NH_4^+. These molecules/ions were described in the same crystallographic site totally occupied, with a ratio N/O = 0.125/1.875 giving better refinement and a charge balance ensured by the ammonium ion, so the formula $(NH_4)_{0.5}[Pu^{III}_{0.5}U^{IV}_{0.5}(C_2O_4)_2(H_2O)]{\cdot}nH_2O$ is proposed, although partial substitution of H_3O^+ for NH_4^+ cannot be ruled out.

The structure of this uranium(IV)/plutonium(III) oxalate (**1**) is similar to that of the *tetragonal* series described in various U^{IV}/Ln^{III} systems[30] and to that of $U^{IV}(C_2O_4)_2{\cdot}H_2O{\cdot}$dma in which neutral dimethylamine molecules occupy the interlayer spaces between the nonsubstituted $[U^{IV}(C_2O_4)_2{\cdot}H_2O]$ layers instead of the monovalent cations.[7] The study of the *tetragonal* U^{IV}/Ln^{III} systems showed that the average U/Ln−O distance is influenced by the largest metal (lanthanide), and a monotonic variation of the average distance with the ionic radius of the Ln^{3+} cation in nine-coordination was obtained.[30] According to ionic radii, M−O distances for the U^{IV}/Pu^{III} system should be close to or even slightly greater than the rate of metal(III), being greater than those of the U^{IV}/Nd^{III} one ($R_{Nd^{III}}$ = 1.163 Å[27] and $R_{Pu^{III}}$ = 1.165(2) Å[28] for CN = 9). Actually, the distances are smaller for the uranium(IV)−plutonium(III) oxalate than for the uranium(IV)−neodymium(III) one and closer to that of uranium(IV) oxalate (Table 2). These results are in agreement with an increase of the covalent contribution to the bonding of actinide(III) complexes relative to similar lanthanide(III) complexes.[32,52,53] Splitting the mixed site into two half-occupied positions does not significantly improved the results. The two positions are separated by 0.19(2) Å and the distances M−O are somewhat different, but the average distances are equal for both sites, which precludes any allocation of sites to U^{IV} and Pu^{III} and any conclusion in the absence of additional experiments such as extended X-ray absorption fine structure (EXAFS) that might help to determine the uranium and plutonium environments.

The structure of **2** can be described as a honeycomb-like arrangement of actinide and oxalate ions. Although the structure is 3D, it is instructional to describe the connection of the actinides in the (0 0 1) plane through three oxalate ions denoted as Ox1 to form a 2D network of six-membered rings further connected in the [0 0 1] direction through Ox2 oxalates

dx.doi.org/10.1021/ic302587t | Inorg. Chem. 2013, 52, 4941−4949

(Figures 8 and 9). The actinide atom is at the center of a trigonal bipyramid formed by the five oxalates with a

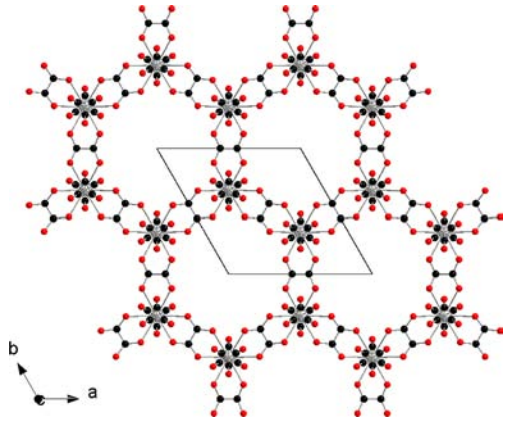

Figure 8. Projection along [0 0 1] of the average structure of **2** showing the honeycomb-like actinide oxalate arrangement.

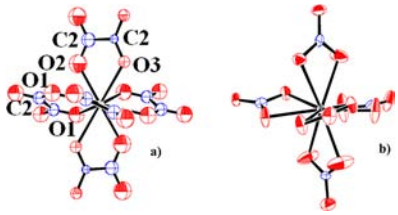

Figure 9. Coordination of the mixed U^{IV}/Pu^{III} site in **2** (a) compared with that of An^{IV} in the $[An(CO_3)_5]^{6-}$ ion polyhedron (b) with atomic numbering in structure **2**.

pseudoaxial arrangement along [0 0 1] of the two oxalates Ox2 and an arrangement of the three oxalates Ox1 approximately perpendicular to this direction. The dihedral angle between the plane Ox2 and the mean plane of the three Ox1 oxalates is 88.1(5)°. A similar geometry is observed for the isolated $[An(CO_3)_5]^{6-}$ ion in actinide carbonates for An = Th[53], U[54], and Pu[55]. In $M_2[(UO_2)_2(C_2O_4)_3]\cdot 4H_2O$ (M = K[56] and NH_4[11]) uranyl oxalates, the two axial oxalates are replaced by the uranyl oxygen atoms. In **2**, the actinide atoms are surrounded by 10 oxygen atoms from three Ox1 and two Ox2 ions acting as μ^2-oxalates. The Ox1 oxalates are disordered on two positions related by the *m* mirror parallel to (0 0 1) while the Ox2 oxalates are disordered on three positions related by the axis parallel to [0 0 1]. The geometry of the $(U,Pu)O_{10}$ polyhedron depends of the exact oxalates involved in coordination of the central metal. Although only an average structure was determined, we can conclude that the mixed uranium–plutonium oxalate framework is similar to that described in $(NH_4)_2U^{IV}_2(C_2O_4)_5\cdot 0.7H_2O$[8] and that this compound belongs to the *hexagonal* series.[8] In the uranium compound, superstructure reflections were observed, allowing determination of the actual structure in a supercell. In compound **2**, in spite of numerous crystals being tested, superstructure reflections were never observed. An average structure was also determined for $(H_3O)_2Np^{IV}_2(C_2O_4)_5\cdot nH_2O$[17] but in the space group *P*3. The *P6/mmm* space group corresponds to the one obtained for the superstructure averaged in the subcell and leads to planar oxalates with actinide atoms within the mean planes and acceptable C–C and C–O distances (Table S4 in the Supporting Information). As for the structure of **1**, the (U,Pu)–O distances within the $(U,Pu)O_{10}$ polyhedron (Table 3) are close to the values calculated for the uranium(IV) oxalate $(NH_4)_2U^{IV}_2(C_2O_4)_5\cdot 0.7H_2O$[8] and uranium(IV) carbonate $Na_6[U^{IV}(CO_3)_5]\cdot 12H_2O$[54–56] and lower than those in the neodymium(III)-substituted oxalate $Na_{2.46}[Nd^{III}_{0.46}U^{IV}_{1.54}(C_2O_4)_5]\cdot 7.6H_2O$,[8] confirming the higher covalence of the Pu^{III}–O bonds compared to the Nd^{III}–O bonds. Because of the disorder in the subcell, the location of the ammonium nitrogen and water oxygen atoms is unrealistic.

CONCLUSION

Single crystals of the mixed uranium(IV) and plutonium(III) oxalates, $(NH_4)_{0.5}[Pu^{III}_{0.5}U^{IV}_{0.5}(C_2O_4)_2\cdot H_2O]\cdot nH_2O$ (**1**) and $(NH_4)_{2.7}Pu^{III}_{0.7}U^{IV}_{1.3}(C_2O_4)_5\cdot nH_2O$ (**2**), have been obtained using a crystal growth method based on the diffusion of species through membranes. The structure of **1** has been completely solved and an average structure for **2** is proposed. The crystal structure studies showed that these compounds are isomorphic to the *tetragonal* and *hexagonal* series of uranium(IV)–lanthanide(III) oxalates previously described.[19] Details of the M–O bonds reveal a higher covalent contribution in the Pu^{III}–O bonds relative to the Nd^{III} ones.

Only powders of mixed uranium(IV)–plutonium(III) oxalate belonging to the *hexagonal* series have been prepared

Table 3. U–O and U/Pu Distances (Å) for 2 Compared with $(NH_4)_2U^{IV}_2(C_2O_4)_5\cdot 0.7H_2O$,[8] $Na_{2.46}[Nd^{III}_{0.46}U^{IV}_{1.54}(C_2O_4)_5]\cdot 7.6H_2O$,[8] and $Na_6[U^{IV}(CO_3)_5]\cdot 12H_2O$[54]

	$(NH_4)_2U^{IV}_2(C_2O_4)_5\cdot 0.7H_2O$		$Na_{2.46}[Nd^{III}_{0.46}U^{IV}_{1.54}(C_2O_4)_5]\cdot 7.6H_2O$		$(NH_4)_{2.7}[Pu^{III}_{0.7}U^{IV}_{1.3}(C_2O_4)_5]\cdot nH_2O$ (**2**)		$Na_6[U^{IV}(CO_3)_5]\cdot 12H_2O$	
U/X^{III}-O(Ox1)	2.507(11)(2x) 2.447(11)(2x) 2.448(15)(2x)	2.467(12)	2.441(8) 2.454(7) 2.486(8) 2.494(8) 2.554(9) 2.562(8)	2.499(8)	2.47(2) (6x)		2.399(5) 2.418(5) 2.434(5) 2.493(6) 2.505(5) 2.515(6)	2.461(5)
U/X^{III}-O(Ox2)	2.462(15)(2x) 2.441(14)(2x)	2.451(15)	2.432(8) 2.475(8) 2.492(8) 2.520(8)	2.480(8)	2.39(4) (2x) 2.50(2) (2x)	2.45(3)	2.411(7) 2.417(6) 2.499(5) 2.517(6)	2.461(6)
<U/X^{III}-O>	2.46(2)		2.491(8)		2.46 (2)		2.461(6)	

dx.doi.org/10.1021/ic302587t | *Inorg. Chem.* 2013, 52, 4941–4949

to date. This study demonstrates, through the crystal growth method developed, the possibility of synthesizing uranium(IV)−plutonium(III) oxalates with the *tetragonal* structure. The existence of this phase opens the possibility of forming mixed uranium−plutonium oxides with higher plutonium content and platelet morphology. Definition of the synthesis conditions to precipitate powder samples of uranium/plutonium tetragonal oxalates and to grow ordered hexagonal uranium/plutonium oxalates is planned. The synthesis of a uranium/plutonium tetragonal oxalate powder will allow further studies of the local actinide environments through EXAFS and powder neutron diffraction experiments.

■ ASSOCIATED CONTENT

Supporting Information

Crystallographic data in CIF format and supplementary tables. This material is available free of charge via the Internet at http://pubs.acs.org.

■ AUTHOR INFORMATION

Corresponding Author

*E-mail: Murielle.rivenet@ensc-lille.fr.

Notes

The authors declare no competing financial interest.

■ ACKNOWLEDGMENTS

This work benefited from the financial support of Agence Nationale de la Recherche (Grant ANR-08-BLAN-0216).

■ REFERENCES

(1) (a) Mew, D. A.; Krikorian, O. H.; Dodson, K. E.; Schmitz, J. A. U.S. Department of Energy, Lawrence Livermore National Laboratory, http://www.osti.gov/bridge/product.biblio.jsp?osti_id=15005300, 2001. (b) Banushali, R. D.; Pius, I. C.; Mukerjee, S. K.; Vaidya, V. N. *J. Radioanal. Nucl. Chem.* **1999**, *240*, 977−979. (c) Grandjean, S., Beres A., Rousselle, J.; Maillard C. World Patent WO 2005/119699, 2005.

(2) Akhtar, M. N.; Smith, A. J. *Acta Crystallogr.* **1975**, *B31*, 1361−1366.

(3) Ziegelgruber, K. L.; Knope, K. E.; Frisch, M.; Cahill, C. L. *J. Solid State Chem.* **2008**, *181*, 373−381.

(4) Favas, M. C.; Kepert, D. L.; Patrick, J. M.; White, A. H. *J. Chem. Soc., Dalton Trans.* **1983**, *3*, 571−581.

(5) Clavier, N.; Hingant, N.; Rivenet, M.; Obbade, S.; Dacheux, N.; Barré, N.; Abraham, F. *Inorg. Chem.* **2010**, *49*, 1921−1931.

(6) (a) Imaz, I.; Bravic, G.; Sutter, J.-P. *Chem. Commun.* **2005**, 993−995. (b) Spirlet, M. R.; Rebizant, J.; Kanellakopulos, B.; Dornberger, E. *Acta Crystallogr.* **1987**, *C43*, 19−21. (c) Imaz, I.; Bravic, G.; Sutter, J.-P. *Dalton Trans.* **2005**, 3681−2687. (d) Mörtl, K. P.; Sutter, J.-P.; Golhen, S.; Ouahab, L.; Kahn, O. *Inorg. Chem.* **2000**, *39*, 1626−1627. (e) Wang, C.-M.; Liao, C.-H.; Chen, P.-L.; Lii, K.-H. *Inorg. Chem.* **2006**, *45*, 1436−1438.

(7) Duvieubourg-Garela, L.; Vigier, N.; Abraham, F.; Grandjean, S. *J. Solid State Chem.* **2008**, *181*, 1899−1908.

(8) Chapelet, B.; Nowogrocki, G.; Abraham, F.; Grandjean, S. *J. Solid State Chem.* **2005**, *178*, 3046−3054.

(9) Wang, C.-M.; Liao, C.-H.; Chen, P.-L.; Lii, K.-H. *Inorg. Chem.* **2006**, *45*, 1436−1438.

(10) (a) Duvieubourg, L.; Nowogrocki, G.; Abraham, F.; Grandjean, S. *J. Solid State Chem.* **2005**, *178*, 3437−3444. (b) Giesting, O. A.; Porter, N. J.; Burns, P. C. *Z. Kristallogr.* **2006**, *221*, 252−269. (c) Baeva, E. E.; Mikhailov, Yu. N.; Gorbunova, Yu. E.; Serezhkina, L. B.; Serezhkin, V. N. *Z. Neorg. Khim.* **2002**, *47*, 1475−1479. (d) Poojary, M. D. *Proc. Indian Acad. Sci. (Chem. Sci)* **1987**, *99*, 311−315. (e) Akhmerkina, Zh. V.; Mikhailov, Yu. N.; Gorbunova, Yu. E.; Serezhkina, L. B.; Serezhkin, V. N. *Z. Neorg. Khim.* **2004**, *49*, 1692−1695. (f) Shilova, M. Yu.; Vologzhanina, A. V.; Serezhkina, L. B.; Serezhkin, V. N. *Z. Neorg. Khim.* **2009**, *54*, 1842−1846. (g) Artem'eva, M. Yu.; Mikhailov, Yu. N.; Gorbunova, Yu. E.; Serezhkina, L. B.; Serezhkin, V. N. *Z. Neorg. Khim.* **2005**, *50*, 1269−1272. (h) Artem'eva, M. Yu.; Mikhailov, Yu. N.; Gorbunova, Yu. E.; Serezhkina, L. B.; Serezhkin, V. N. *Z. Neorg. Khim.* **2003**, *48*, 1473−1475. (i) Thuéry, P. *Polyhedron* **2007**, *26*, 101−106. (j) Legros, J.-P.; Jeannin, Y. *Acta Crystallogr.* **1976**, *B32*, 2497−2503. (k) Govindarajan, S.; Patil, H. C.; Poojary, M. D.; Manoha, H. *Inorg. Chim. Acta* **1986**, *120*, 103−107. (l) Chumaevskii, N. A.; Minaeva, N. A.; Mikhailov, Yu. N.; Gorbunova, Yu. E.; Beirakhov, A. G.; Shchelokov, R. N. *Z. Neorg. Khim.* **1998**, *43*, 789−795. (m) Alcock, W. *J. Chem. Soc., Dalton Trans.* **1973**, 1614−1615. (n) Alcock, W. *J. Chem. Soc., Dalton Trans.* **1973**, 1616−1619. (o) Jayadevan, N. C.; Mudher, K. D. S.; Chackraburtty, D. M. *Acta Crystallogr.* **1975**, *B31*, 2277−2280. (p) Alcock, W. *J. Chem. Soc., Dalton Trans.* **1973**, 1610−1613. (q) Baeva, E. E.; Mikhailov, Yu. N.; Gorbunova, Yu. E.; Serezhkina, L. B.; Serezhkin, V. N. *Z. Neorg. Khim.* **2003**, *48*, 1801−1807.

(11) Chapelet-Arab, B.; Nowogrocki, G.; Abraham, F.; Grandjean, S. *Radiochim. Acta* **2005**, *93*, 279−286.

(12) (a) Tomilin, S. *Radiokhimiya* **1984**, *26*, 734−739. (b) Grigor'ev, M. S.; Baturin, N. A.; Regel', L. L.; Krot, N. N. *Radiokhimiya* **1991**, *33*, 19−25. (c) Charushnikova, I. A.; Krot, N. N.; Polyakova, I. N. *Radiochemistry* **2005**, *47*, 495−499. (d) Charushnikova, I. A.; Krot, N. N.; Polyakova, I. N. *Radiochemistry* **2006**, *48*, 223−226. (e) Bean, A. C.; Garcia, E.; Scott, B. L.; Runde, W. *Inorg. Chem.* **2004**, *43*, 6145−6147. (f) Krot, N. N.; Bessonov, A. A.; Charushnikova, I. A.; Makarenkov, V. I. *Radiochemistry* **2007**, *49*, 107−111.

(13) Jenkis, I. L.; Moore, F. H.; Waterman, M. J. *J. Inorg. Nucl. Chem.* **1965**, *27*, 77−80.

(14) Weigel, F.; Meer, N. *Inorg. Nucl. Chem. Lett.* **1967**, *3*, 403−407.

(15) Grigoriev, M. S.; Charushnikova, I. A.; Krot, N. N.; Yanovskii, A. I.; Struchkov, Y. T. *Radiochemistry* **1997**, *39*, 420−423.

(16) Vigier, N.; Grandjean, S.; Arab-Chapelet, B.; Abraham, F. *J. Alloys Compd.* **2007**, *444*, 594−597.

(17) Charushnikova, I. A.; Krot, N. N.; Katser, S. B. *Radiochemistry* **1998**, *40*, 558−564.

(18) Andreev, G. B.; Budantseva, N. A.; Fedoseev, A. M.; Moisy, Ph. *Inorg. Chem.* **2011**, *50*, 11481−11486.

(19) Runde, W.; Brodnax, L. F.; Bean, A.; Scott, B. L. *Inorg. Chem.* **2009**, *4*, 5967−5972.

(20) Ollendorff, W.; Weigel, F. *Inorg. Nucl. Chem. Lett.* **1969**, *5*, 263−269.

(21) Hernandez-Molina, M.; Lorenzo-Luis, P. A.; Ruiz-Perez, C. *CrystEngComm* **2001**, *16*, 1−4.

(22) Chapelet-Arab, B.; Grandjean, S.; Nowogrocki, G.; Abraham, F. *J. Alloys Compd.* **2007**, *444*−*445*, 387−390.

(23) Grandjean, S.; Arab-Chapelet, B.; Bertrand, M.; Picart, S.; Baron, P.; Blanc, P.; Warin, D. *Proceedings of Global 2009*, Paris, France, Sept 6−11, 2009; Paper 9441.

(24) Grandjean, S.; Arab-Chapelet, B.; Robisson, A.-C.; Abraham, F.; Martin, Ph.; Dancausse, J.-Ph.; Herlet, N.; Léorier, C. *J. Nucl. Mater.* **2009**, *385*, 204−207.

(25) Arab-Chapelet, B.; Grandjean, S.; Nowogrocki, G.; Abraham, F. *J. Nucl. Mater.* **2008**, *373*, 259−268.

(26) Horlait, D.; Clavier, N.; Dacheux, N.; Cavalier, R.; Podor, R. *Mater. Res. Bull.* **2012**, *47*, 4017−4025.

(27) Shannon, R. D. *Acta Crystallogr.* **1976**, *A32*, 751−767.

(28) Cross, J. N.; Villa, E. M.; Wang, S.; Diwu, J.; Polinski, M. J.; Albrecht-Schmitt, T. E. *Inorg. Chem.* **2012**, *51*, 8419−8424.

(29) Chapelet-Arab, B.; Nowogrocki, G.; Abraham, F.; Grandjean, S. *J. Solid State Chem.* **2005**, *178*, 3055−3065.

(30) Chapelet-Arab, B.; Duvieubourg, L.; Nowogrocki, G.; Abraham, F.; Grandjean, S. *J. Solid State Chem.* **2006**, *179*, 4029−4036.

(31) Polinski, M. J.; Grant, D. J.; Wang, S.; Alekseev, E. V.; Cross, J. N.; Villa, E. M.; Depmeier, W.; Gagliardi, L.; Albrecht-Schmitt, T. E. *J. Am. Chem. Soc.* **2012**, *134*, 10682−10692.

(32) Polinski, M. J.; Wang, S.; Cross, J. N.; Alekseev, E. V.; Depmeier, W.; Albrecht-Schmitt, T. E. *Inorg. Chem.* **2012**, *51*, 7859−7866.

(33) (a) Szigethy, G.; Xu, J.; Gorden, A. E. V.; Teat, S. J.; Shuh, D. K.; Raymond, K. N. *Eur. J. Inorg. Chem.* **2008**, *13*, 2143. (b) Diwu, J.; Wang, S.; Liao, Z.; Burns, P. C.; Albrecht-Schmitt, T. E. *Inorg. Chem.* **2010**, *49*, 10074−10080. (c) Diwu, J.; Wang, S.; Good, J.; Di Stefano, V. H.; Albrecht-Schmitt, T. E. *Inorg. Chem.* **2011**, *50*, 4842−4850. (d) Cross, J. N.; Duncan, P. M.; Villa, E. M.; Polinski, M. J.; Babo, J.-M.; Alekseev, E. V.; Booth, C. H.; Albrecht-Schmitt, T. E. *J. Am. Chem. Soc.* **2013**, *135*, 2769−2765.
(34) Tamain, C.; Arab-Chapelet, B.; Rivenet, M.; Grandjean, S.; Abraham, F. *Cryst. Growth Des.* **2012**, *12*, 5447−5455.
(35) *SAINTPlus*, version 6.22; Bruker Analytical X-ray Systems: Madison, WI, 2001.
(36) *SADABS*, version 2.03; Bruker Analytical X-ray Systems: Madison, WI, 2001.
(37) Petricek, V. Dusek, M. Palatinus, L.*JANA2000, Crystallographic Computing System for Standard and Modulated Structures*; Institute of Physics: Prague, Czech Republic, 2000.
(38) Altomare, M. C. Burla, M. Camalli, G. Cascarano, C. Giacovazzo, A. Guagliardi, A. G. G. Moliterni, G. Polidori, R. *SIR97: a New Program For Solving and Refining Crystal Structures*; 1997.
(39) *DIFFRAC^{plus} EVA*; Bruker AXS: Karlsruhe, Germany, 2007.
(40) (a) Clark, D. L.; Hecker, S. S.; Jarvinen, G. D.; Neu, M. P.Plutonium. *The Chemistry of Actinides and Transactinides Elements*, 3rd ed.; Springer: Dordrecht, The Netherlands, 2008; Chapter 7. (b) Gourisse, D.; Madic, C. *Gmelin Handbuch des Anorganischen Chemie*; Sprinker-Verlag: Berlin, 1975; pp 27−29. (c) Mesmin, C.; Hanssens, A.; Blanc, P.; Madic C.; Debreuille, M. F. World Patent WO/2002/028778, 2002.
(41) (a) Chung, D. Y.; Kim, E. H.; Lee, E. H.; Yoo, J. H. *Ind. Eng. Chem.* **1998**, *4*, 277−284. (b) Gel'man, A. D.; Matorina, N. N.; Moskvin, A. I. *Sov. At. Energy* **1957**, *3*, 1115−1120. (c) Zakolupin, S. A.; Korablin, E. V. *Sov. Radiochem.* **1977**, *3*, 581−584.
(42) (a) Moskvin, A. I.; Gel'man, A. *Russ. J. Inorg. Chem.* **1958**, *3*, 198−216. (b) Moskvin, A. I.; Essen, L. N. *Russ. J. Inorg. Chem.* **1967**, *12*, 359−362. (c) Zakharova, F. A.; Moskvin, A. I. *Russ. J. Inorg. Chem.* **1960**, *5*, 592−595.
(43) (a) Moskvin, A. I.; Zakharova, F. A. *Russ. J. Inorg. Chem.* **1959**, *4*, 975−979. (b) Drabkina, L. E.; Moskvin, A. I.; Gel'man, A. D. *Russ. J. Inorg. Chem.* **1958**, *3*, 290−294.
(44) (a) Edwards, H. G. M.; Russell, N. C.; Seaward, M. R. D. *Spectrochim. Acta* **1997**, *A53* (1), 99−105. (b) Frost, R. L.; Weier, M. L. *J. Raman Spectrosc.* **2003**, *34* (10), 776−785. (c) Frost, R. L.; Adebajo, M.; Weier, M. L. *Spectrochim. Acta* **2004**, *A60* (3), 643−651. (d) D'Antonio, M. C.; Palacios, D.; Coggiola, L.; Baran, E. J. *Spectrochim. Acta* **2007**, *A68* (3), 424−426. (e) Duval, D.; Condrate, R. A. *Appl. Spectrosc.* **1988**, *42* (4), 701−702.
(45) Hingant, N.; Clavier, N.; Dacheux, N.; Barre, N.; Hubert, S.; Obbade, S.; Taborda, F.; Abraham, F. *J. Nucl. Mater.* **2009**, *385*, 400−406.
(46) Kanno, H.; Hiraishi, J. *J. Phys. Chem.* **1984**, *88*, 2787−2792. Lewis, I. R.; Edwards, H. G. M. *Handbook of Raman Spectroscopy*; Marcel Dekker: New York, 2001.
(47) Runde, W.; Neu, M. P.; Van Pelt, C.; Scott, B. L. *Inorg. Chem.* **2000**, *39*, 1050−1051.
(48) (a) Goff, G. S.; Cisneros, M. R.; Kluk, C.; Williamson, K.; Scott, B. L.; Reilly, S.; Runde, W. *Inorg. Chem.* **2010**, *49*, 6558−6564. (b) Janicki, R.; Starynowicz, P.; Mondry, A. *Eur. J. Inorg. Chem.* **2011**, 3601−3616.
(49) Burns, C. J.; Neu, M. P.; Boukhalfa, H.; Gutowski, K. E.; Bridges, N. J.; Rogers, R. D. *Compr. Coord. Chem. II* **2004**, *3*, 189−345.
(50) (a) McDonald, T. R. R.; Spink, J. M. *Acta Crystallogr.* **1967**, *23*, 944−949. (b) Brunton, G. D.; Johnson, C. K. *J. Chem. Phys.* **1975**, *62*, 3797−3806. (c) Trombe, J. C.; Thomas, P.; Brouca-Cabarrecq, C. *Solid State Sci.* **2001**, *3*, 309−319. (d) Fourcade-Cavillon, F.; Trombe, J. C. *Solid State Sci.* **2002**, *4*, 1199−1208. (e) Bataille, T.; Auffrédic, J. P.; Louër, D. *J. Mater. Chem.* **2000**, *10*, 1707−1711. (f) Bataille, T.; Louër, D. *Acta Crystallogr.* **1999**, *C55*, 1760−1762.
(51) Hahn, T. *Z. Anorg. Allg. Chem.* **1957**, *109*, 438−466.
(52) Gaunt, A. J.; Reilly, S. D.; Enriquez, A. E.; Scott, B. L.; Ibers, J. A.; Sekar, P.; Ingram, K. I. M.; Kaltsoyannis, N.; Neu, M. P. *Inorg. Chem.* **2008**, *47*, 29−41.
(53) (a) Violitis, S.; Rimsky, A. *Acta Crystallogr.* **1975**, *B31*, 2612−2615. (b) Violitis, S.; Rimsky, A. *Acta Crystallogr.* **1975**, *B31*, 2615−2620.
(54) Hennig, C.; Ikeda-Ohno, A.; Emmerling, F.; Kraus, W.; Bernhard, G. *Dalton Trans.* **2010**, *39*, 3744−3750.
(55) Clark, D. L.; Conradson, S. D.; Keogh, D. W.; Palmer, P. D.; Scott, B. L.; Tait, C. D. *Inorg. Chem.* **1998**, *37*, 2893−2899.
(56) Jayadevan, N. C.; Mudher, K. D. S.; Chackraburtty, D. M. *Acta Crystallogr.* **1975**, *B31*, 2277−2280.